

Machine Learning for LiDAR-Based Navigation System

Farhad Aghili*

Abstract

This paper presents a robust 6-DOF relative navigation by combining the iterative closet point (ICP) registration algorithm and a noise-adaptive Kalman filter (AKF) in a closed-loop configuration together with measurements from a laser scanner and an inertial measurement unit (IMU). In this approach, the fine-alignment phase of the registration is integrated with the filter innovation step for estimation correction while the filter estimate propagation provides the coarse alignment needed to find the corresponding points at the beginning of ICP iteration cycle. The convergence of the ICP point matching is monitored by a fault-detection logic and the covariance associated with the ICP alignment error is estimated by a recursive algorithm. This ICP enhancement has proven to improve robustness and accuracy of the pose tracking performance and to automatically recover correct alignment whenever the tracking is lost. The Kalman filter estimator is designed so as to identify the required parameters such as IMU biases and location of the spacecraft center-of-mass (CoM).

1 Introduction

Robust relative navigation systems are critical for many current and near-future lunar or space exploration missions to support rendezvous, proximity operations and docking for both crewed and un-crewed vehicles [1, 2, 3]. Fault-tolerant is a vital design requirement in development of relative navigation systems for these aerospace applications. In particular, reliable relative pose information in full 6-dof is required during approach and docking operations for visiting vehicles with the International Space Station (ISS). It is deemed that the safety of the controlled spacecraft during such proximity maneuvers critically depends on the performance and robustness of the relative navigation systems. Failure of relative navigation systems to provide continuous and accurate pose (position and orientation) is considered as a critical hazard or even a catastrophic hazard that can cause failure of the mission all together.

There are different relative navigation sensors capable of estimating the pose of objects having relative motion. Application of radar and altimetry for space-borne navigation systems began more than half a century ago [4], while X-ray pulsars for relative navigation between two spacecraft in deep space is recently presented [5, 6, 7, 8]. Other relative navigation methods focus on using Global Position System (GPS) for determining both absolute and relative position and attitude between two spacecraft [9, 10, 11, 12, 13]. There are also different vision systems capable of estimating the pose of two objects moving with respect to each other

*email:faghili@encs.concordia.ca

[14, 15, 16, 17, 18]. Although using radar or GPS for relative navigation systems are with the advantage of long-range distance measurement, they are with less resolution and precision compared with the vision-based systems. Moreover, the advent of relatively low-cost and commercially available laser range sensors and scanners, which has been greatly exploited for autonomous navigation of robotic vehicles [19, 20, 21, 22, 23, 24, 25, 26], makes them preferred sensor of choice in relative navigation systems. Moreover, it has been shown that laser scanners exhibit acceptable robustness in the face of the harsh lighting conditions of space. For instance, a rendezvous laser sensor was used as the primary navigation to perform unmanned autonomous rendezvous docking experiments in the ETS-VII mission [16]. Vision algorithms for laser scanners have been also developed for motion estimation of free-floating objects to support a variety of on-orbit proximity operations [14, 27, 28, 29, 17, 30, 31, 32]. However, fault tolerance capability is not incorporated in these vision algorithms to achieve robust pose-tracking performance.

The conventional vision-based pose estimation algorithms are essentially 3D registration processes, by which the range data set from different views are aligned in a common coordinate system [33]. The iterative closest point (ICP) is the cornerstone of 3D vision-based pose estimation algorithm and one of the most popular registration methods. The iterative procedure minimizes a distance between point cloud in one dataset and the closest points in the other [34, 35]. Typically, one dataset is a set of 3D point-cloud acquired by scanning an object, while the other one is a model set such as a CAD model of the same object. The basic ICP algorithm has proven to be very useful in the processing of range data [35] and subsequently a number of variations on the basic method have been developed to optimize different phases of the algorithm [36, 37, 38, 35]. Recently, several improved algorithms of ICP by adopting Lie groups have been reported in the literature [39, 40]. The advantage of these algorithms is that it converges monotonically to a local minimum from any given initial parameters. Although the modified ICP algorithms improve the convergence to local minima and sensitivity to outliers and disturbances, they still suffer from slow convergence or even divergence if proper initial pose estimate is not available [41]. Other registration methods include tangent-squared distance minimization (TDM) [42], squared distance minimization (SDM) [43], and adaptive distance function (ADF) [41]. Although point-tangent methods, i.e., TDM and SDM, reportedly exhibit faster convergent rate than ICP does [42], they have their own drawbacks. For instance, the efficiency of SDM algorithm is compromised by the heavy computation required to get the curvature value of each discrete point, while TDM requires a good initial estimate of initial pose otherwise registration may fail in iteration [41]. The shortest distance is more generally defined in the ADF method than in the other traditional methods. In fact, by varying a scalar coefficient, the ADF distance function can be turned into the point-tangent distance function of TDM or the point-point distance function of ICP [41]. This means that TDM and ICP methods are actually special cases of the ADF. Therefore, the ADF algorithm has the potential to get a compromised performance with faster convergence rate of ICP and improved robustness of TDM [41].

It is known that the registration algorithms are not guaranteed to converge to a global minimum unless the initial alignment is sufficiently close to the actual one. More specifically, convergence of ICP iteration and the accuracy of the fine-alignment process depend on quality of the 3-D vision data that can be adversely affected by many factors such as sensor noise, disturbance, outliers, symmetric view of the target, or incomplete scan data. Taking advantage

of the simple dynamics of a free-floating object, which is not acted upon by any external force or moment, researchers have employed different observers to track and predict the motion of free-floating space objects [44, 17, 9]. However, relative thrust acceleration was not accounted for in these methods and therefore they are not applicable for relative navigation. In this work, a relative navigation is developed by incorporating the dynamics model of the relative pose in the ICP algorithm to improve the accuracy, performance, and robustness of the overall pose estimation process. Measurement from onboard IMU accounts for relative thrust acceleration making the pose estimation suitable for relative navigation applications. As depicted in Fig. 1, robustness in pose tracking is achieved by integration of ICP and an adaptive Kalman filter using a fault-detection logic. Here, the state estimation is updated with the value of the fine-alignment as soon as the ICP succeeds to match the points, while the predicted pose obtained at the propagation estimate step of the filter gives the coarse alignment required to find the corresponding points. A recursive algorithm updates the covariance estimate associated with the fine-alignment error at every time step. This information along with detection of ICP convergence by the fault-detection logic are used to adaptively tune the Kalman filter for reliable estimation of the motion states together with a set of relevant parameters, e.g., IMU bias and spacecraft CoM. It is proven experimentally that this closed-loop ICP-AKF architecture, in which the ICP initial guess is continually provided by the dynamic predictor, establishes robust pose tracking and allows automatic fault recovery. Moreover, the computation time can be improved because of the better initial guess and hence less ICP iterations would be usually required. The robustness and accuracy performance of the relative navigation are tested in a robotic experimental setup. In it, the mock-up of a spacecraft attached to a robotic arm, which is driven by a simulator to produce the relative motion dynamics between two objects in orbit. The spacecraft mockup is then scanned by a laser range sensor while the mockup is in motion and subsequently 3-D scan data is fed to our relative navigation system in real-time.

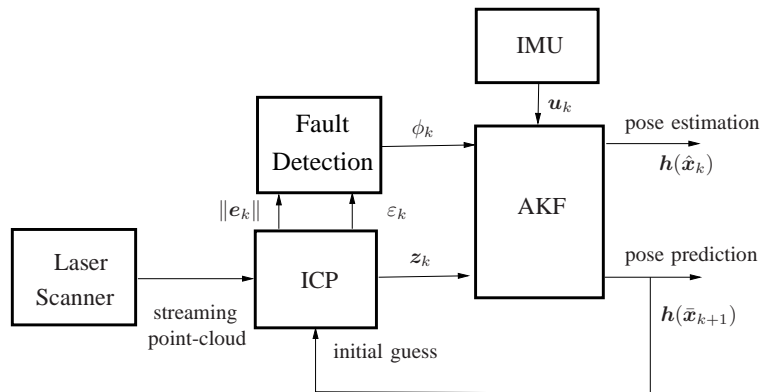


Figure 1: Architecture of the robust relative navigation.

2 Dynamics Model

Consider a target spacecraft, namely the Space Station, and a docking spacecraft and as rigid bodies moving in nearby orbits. We assume that a laser scanner sensor and an IMU are installed on the docking vehicle so that they provide 3-D range data of the preceding spacecraft as well as

the acceleration thrust during orbital maneuvers performed in a space rendezvous and docking. Coordinate frames $\{\mathcal{A}\}$ and $\{\mathcal{B}\}$ are attached to bodies of the docking and target spacecraft, respectively. The origins of frames $\{\mathcal{A}\}$ and $\{\mathcal{B}\}$ are located at CoMs of the corresponding spacecraft. Coordinate frame $\{\mathcal{B}\}$ is orientated so that its y -axis is parallel to a line connecting the Earth's center to the spacecraft CoM and pointing outward, and its x -axis lies on the orbital plane. Without loss of generality, we assume that the coordinate frame, $\{\mathcal{A}\}$, coincides with the coordinate frame of the on-board IMU.

The relative attitude of the docking spacecraft with respect to the target spacecraft, which is called the Station hereafter, is presented by quaternion \mathbf{q} , but the attitude-control system of the Station makes it rotate with the angular velocity of the reference orbit. The rotation matrix \mathbf{A} corresponding to the quaternion \mathbf{q} is given by the following expression

$$\mathbf{A}(\mathbf{q}) = (2q_o^2 - 1)\mathbf{I} + 2q_o[\mathbf{q}_v \times] + 2\mathbf{q}_v \mathbf{q}_v^T, \quad (1)$$

where \mathbf{q}_v and q_o are the vector and scalar parts of the quaternion, i.e., $\mathbf{q} = [\mathbf{q}_v^T \ q_o]^T$, $[\cdot \times]$ denotes the matrix form of the cross-product, and \mathbf{I} denotes identity matrix with adequate dimension. The quaternion product \otimes is defined as

$$\mathbf{q} \otimes = q_o \mathbf{I} + \boldsymbol{\Omega}(\mathbf{q}_v) \quad \text{where} \quad \boldsymbol{\Omega}(\mathbf{q}_v) = \begin{bmatrix} -[\mathbf{q}_v \times] & \mathbf{q}_v \\ -\mathbf{q}_v^T & 0 \end{bmatrix}$$

so that $\mathbf{q}_1 \otimes \mathbf{q}_2$ corresponds to rotation matrix $\mathbf{A}(\mathbf{q}_2)\mathbf{A}(\mathbf{q}_1)$.

Assume that displacement vectors $\boldsymbol{\rho}_1$ and $\boldsymbol{\rho}_2$, respectively, represent location of the laser camera in the docking spacecraft w.r.t. its CoM and location of the point of interest on the Station w.r.t. its own CoM and that the displacement vectors are expressed in their corresponding body-attached frames. Also, let us define position vectors $\boldsymbol{\rho}$ and \mathbf{r} as the range of the Station w.r.t. the docking spacecraft expressed in $\{\mathcal{A}\}$ and the relative distance between the CoMs of two spacecraft expressed in $\{\mathcal{B}\}$, respectively. Then, the following kinematics relation is in order

$$\boldsymbol{\rho} = \mathbf{A}^T(\mathbf{r} - \boldsymbol{\rho}_2) + \boldsymbol{\rho}_1, \quad (2)$$

where \mathbf{A} is the rotation matrix from $\{\mathcal{A}\}$ to $\{\mathcal{B}\}$. Considering the visiting spacecraft in the vicinity of the Station, one can describe the evolution of the relative position of the two spacecraft by *orbital mechanics* [45]. The thrust-acceleration measurements of the docking spacecraft \mathbf{a} are provided by IMU. That is

$$\mathbf{a} = \mathbf{u}_a + \mathbf{b}_a + \boldsymbol{\epsilon}_a \quad (3)$$

where \mathbf{u}_a is acceleration measurement output, \mathbf{b}_a is the bias of the accelerometer, and $\boldsymbol{\epsilon}_a$ is the accelerometer noise, which is assumed to be random walk noise with covariance $E[\boldsymbol{\epsilon}_a \boldsymbol{\epsilon}_a^T] = \sigma_a^2 \mathbf{I}$. As shown in the figure, \mathbf{r}_e is the vector position connecting the Earth center to the Station's CoM that is expressed in the frame $\{\mathcal{B}\}$. Suppose vector $\mathbf{n} = n\mathbf{k}$, where $\mathbf{k} = [0 \ 0 \ 1]^T$, denote the angular rate of the Station orbit and hence the angular rate of the rotating frame $\{\mathcal{B}\}$. Then, the relative translational motion of the CoMs expressed in frame $\{\mathcal{B}\}$ can be described by

$$\begin{aligned} \ddot{\mathbf{r}} = & -2\mathbf{n} \times \dot{\mathbf{r}} - \mathbf{n} \times (\mathbf{n} \times \mathbf{r}) - \dot{\mathbf{n}} \times \mathbf{r} \\ & + \mu \left(\frac{\mathbf{r}_e}{\|\mathbf{r}_e\|^3} - \frac{\mathbf{r}_e + \mathbf{r}}{\|\mathbf{r}_e + \mathbf{r}\|^3} \right) + \mathbf{A}(\mathbf{q})(\mathbf{u}_a + \mathbf{b}_a + \boldsymbol{\epsilon}_a), \end{aligned} \quad (4)$$

where $\mu = 3.98 \times 10^{14} \text{ m}^3/\text{s}^2$ is the gravitational parameter of the Earth.

Suppose underlined form of vector $\boldsymbol{\alpha} \in \mathbb{R}^3$ denotes the representation of that vector in \mathbb{R}^4 , e.g., $\underline{\boldsymbol{\alpha}}^T \triangleq [\boldsymbol{\alpha}^T \ 0]$. By virtue of this notation, the time-derivative of the quaternion can be expressed by

$$\dot{\boldsymbol{q}} = \frac{1}{2} \underline{\boldsymbol{\omega}}_{\text{rel}} \otimes \boldsymbol{q}, \quad (5)$$

where $\boldsymbol{\omega}_{\text{rel}} = \boldsymbol{\omega} - \boldsymbol{\omega}_o$ is the relative angular velocity, $\boldsymbol{\omega}_o$ is the angular velocity of the station expressed in frame $\{\mathcal{B}\}$, and $\boldsymbol{\omega}$ is the actual angular rate of the docking spacecraft. The expression of the latter angular velocity is given by

$$\boldsymbol{\omega} = \boldsymbol{u}_g + \boldsymbol{b}_g + \boldsymbol{\epsilon}_g \quad (6)$$

where \boldsymbol{u}_g is the output of gyro, vector \boldsymbol{b}_g is the gyro bias, and $\boldsymbol{\epsilon}_g$ is the gyro noise with covariance $E[\boldsymbol{\epsilon}_g \boldsymbol{\epsilon}_g^T] = \sigma_g^2 \boldsymbol{I}$. The time-derivative of gyro bias is traditionally modeled with random walk model [46, 47] according to

$$\dot{\boldsymbol{b}}_g = \boldsymbol{\epsilon}_b, \quad (7)$$

where $\boldsymbol{\epsilon}_b$ is the rate random walk noise with covariance $E[\boldsymbol{\epsilon}_b \boldsymbol{\epsilon}_b^T] = \sigma_b^2 \boldsymbol{I}_3$. Furthermore, one can relate \boldsymbol{n} and $\boldsymbol{\omega}_o$ using the quaternion transformation [48] as follow

$$\underline{\boldsymbol{\omega}}_o = \boldsymbol{q} \otimes \underline{\boldsymbol{n}} \otimes \boldsymbol{q}^*. \quad (8)$$

where \boldsymbol{q}^* is the conjugate quaternion of \boldsymbol{q} such that $\boldsymbol{q}^* \otimes \boldsymbol{q} = \boldsymbol{q} \otimes \boldsymbol{q}^* = [0 \ 0 \ 0 \ 1]^T$. Then substituting (8) into (5) and using the properties of the quaternion products, we arrive at

$$\begin{aligned} \dot{\boldsymbol{q}} &= \frac{1}{2} \underline{\boldsymbol{\omega}} \otimes \boldsymbol{q} - \frac{1}{2} (\boldsymbol{q} \otimes \underline{\boldsymbol{n}}) \otimes (\boldsymbol{q}^* \otimes \boldsymbol{q}) \\ &= \frac{1}{2} \underline{\boldsymbol{\omega}} \otimes \boldsymbol{q} - \frac{1}{2} \boldsymbol{q} \otimes \underline{\boldsymbol{n}} \\ &= \frac{1}{2} \boldsymbol{\Omega}(\boldsymbol{u}_g + \boldsymbol{b}_g + \boldsymbol{\epsilon}_g) - \frac{1}{2} \boldsymbol{q} \otimes \underline{\boldsymbol{n}} \end{aligned} \quad (9)$$

Now, let us suppose that the parameters remain constant during the estimation process, i.e.,

$$\dot{\boldsymbol{b}}_a = \dot{\boldsymbol{\rho}}_1 = \dot{\boldsymbol{\rho}}_2 = \mathbf{0} \quad (10)$$

Then, equations (4), (10), and (9) can be combined in the following standard form

$$\dot{\boldsymbol{x}} = \boldsymbol{f}(\boldsymbol{x}, \boldsymbol{u}, \boldsymbol{\epsilon}) \quad (11)$$

in which vector $\boldsymbol{u} = [\boldsymbol{u}_a^T \ \boldsymbol{u}_g^T]^T$ contains the IMU outputs, vectors $\boldsymbol{\epsilon} = [\boldsymbol{\epsilon}_a^T \ \boldsymbol{\epsilon}_g^T \ \boldsymbol{\epsilon}_b^T]^T$ contains the entire process noise, and

$$\boldsymbol{f}(\boldsymbol{x}, \boldsymbol{u}, \boldsymbol{\epsilon}) = \begin{bmatrix} \dot{\boldsymbol{r}} \\ -2\boldsymbol{n} \times \dot{\boldsymbol{r}} + \boldsymbol{\psi}(\boldsymbol{r}) + \boldsymbol{A}(\boldsymbol{q})(\boldsymbol{u}_a + \boldsymbol{b}_a + \boldsymbol{\epsilon}_a) \\ \frac{1}{2} \boldsymbol{\Omega}(\boldsymbol{u}_g + \boldsymbol{b}_g + \boldsymbol{\epsilon}_g) \boldsymbol{q} - \frac{1}{2} \boldsymbol{q} \otimes \underline{\boldsymbol{n}} \\ \boldsymbol{\epsilon}_b \\ \mathbf{0}_{9 \times 1} \end{bmatrix}$$

Here, the nonlinear function $\boldsymbol{\psi}(\mathbf{r})$ arises from relative acceleration due to effects of orbital mechanics and rotating frame

$$\boldsymbol{\psi}(\mathbf{r}) = \mu \left(\frac{\mathbf{r}_e}{\|\mathbf{r}_e\|^3} - \frac{\mathbf{r} + \mathbf{r}_e}{\|\mathbf{r} + \mathbf{r}_e\|^3} \right) - \mathbf{n} \times (\mathbf{n} \times \mathbf{r}) - \dot{\mathbf{n}} \times \mathbf{r}$$

Note that the gyro and accelerometer measurement noises render the entire process noise and therefore $E[\boldsymbol{\epsilon}\boldsymbol{\epsilon}^T] = \boldsymbol{\Sigma}_{\text{IMU}} = \text{diag}(\sigma_a^2 \mathbf{I}, \sigma_g^2 \mathbf{I}, \sigma_b^2 \mathbf{I})$.

2.1 Linearization

Linearized dynamic model is predominantly used in a variety of navigation systems across both scientific and engineering realms, especially in aerospace. Relative navigation estimators are typically built upon linearized models, e.g., the extended Kalman filter and, to a much lesser extent, the unscented Kalman filter [49]. This is because, in practice, it is sufficient to capture the effects of the relatively small linearization error as a process noise in the state estimation process [50].

Assuming $\|\mathbf{r}\| \ll \|\mathbf{r}_e\|$, one can obtain approximating equation of the orbital mechanics that is *linear* in \mathbf{r} , i.e.,

$$\boldsymbol{\psi}(\mathbf{r}) \approx \boldsymbol{\Gamma} \mathbf{r} \quad (12)$$

where

$$\begin{aligned} \boldsymbol{\Gamma} &= \left. \frac{\partial \boldsymbol{\psi}}{\partial \mathbf{r}} \right|_{\mathbf{r}=0} = -\frac{\mu}{\|\mathbf{r}_e\|^3} \left(\mathbf{I} - 3 \frac{\mathbf{r}_e \mathbf{r}_e^T}{\|\mathbf{r}_e\|^2} \right) - [\mathbf{n} \times]^2 - [\dot{\mathbf{n}} \times] \\ &= \frac{\mu}{\|\mathbf{r}_e\|^3} (2\mathbf{I} + 3[\mathbf{j} \times]^2) - n^2 [\mathbf{k} \times]^2 - \dot{n} [\mathbf{k} \times] \end{aligned} \quad (13)$$

and $\mathbf{j} = \mathbf{r}_e / \|\mathbf{r}_e\|$ is the direction cosine. For a *circular* orbit we have $\dot{\mathbf{n}} = 0$ and the pertinent equation becomes

$$n^2 r_e^3 = \mu$$

Furthermore, if we choose coordinate frame $\{\mathcal{B}\}$ such that $\mathbf{j} = [0 \ 1 \ 0]^T$, then expression of the jacobian matrix in (13) is greatly simplified to

$$\boldsymbol{\Gamma} = \text{diag}(0, 3n^2, -n^2)$$

Although the states can be propagated by solving the nonlinear dynamics equations (11), the state transition matrix of the linearized dynamics equations will be also needed to be used for covariance propagation of the KF. Since additive error quaternion does not lead to a unit vector, a quaternion variation $\tilde{\mathbf{q}}$ using a multiplication error quaternion involving *a posterior* quaternion $\bar{\mathbf{q}}$ is considered for state estimation so that $\tilde{\mathbf{q}} \otimes \bar{\mathbf{q}} = \mathbf{q}$, or equivalently

$$\tilde{\mathbf{q}} = \mathbf{q} \otimes \bar{\mathbf{q}}^*. \quad (14)$$

Assuming small \mathbf{b}_g and $\boldsymbol{\epsilon}_g$, one can adopt a linearization technique similar to [46, 47] to linearize (5) about the quaternion $\bar{\mathbf{q}}$ and angular velocity $\hat{\boldsymbol{\omega}} = \hat{\mathbf{u}}_g + \hat{\mathbf{b}}_g$

$$\frac{d}{dt} \tilde{\mathbf{q}}_v = -\hat{\boldsymbol{\omega}} \times \tilde{\mathbf{q}}_v + \frac{1}{2} (\mathbf{b}_g - \hat{\mathbf{b}}_g) + \frac{1}{2} \boldsymbol{\epsilon}_g \quad (15)$$

Since \tilde{q}_o is not an independent variable and it has variations of only the second order, its time-derivative can be ignored, as suggested in [46]. Moreover, it can be seen from (1) that for small rotation $\tilde{\mathbf{q}}$, where $\|\tilde{\mathbf{q}}_v\| \ll 1$, we have $\mathbf{A}(\tilde{\mathbf{q}}) = \mathbf{I} + 2[\tilde{\mathbf{q}}_v \times]$ and thus

$$\mathbf{A}(\mathbf{q}) \approx \bar{\mathbf{A}}(\mathbf{I} + 2[\tilde{\mathbf{q}}_v \times]) \quad (16)$$

where $\bar{\mathbf{A}} = \mathbf{A}(\bar{\mathbf{q}})$. Now the equation of translational motion (4) can be linearized about the acceleration estimation $\hat{\mathbf{u}}_a + \hat{\mathbf{b}}_a$ and a *posterior* quaternion $\bar{\mathbf{q}}$ using the first-order approximation (16) as:

$$\begin{aligned} \ddot{\mathbf{r}} \approx & -2\mathbf{n} \times \dot{\mathbf{r}} + \mathbf{\Gamma}\mathbf{r} - 2\bar{\mathbf{A}}((\hat{\mathbf{u}}_a + \hat{\mathbf{b}}_a) \times \tilde{\mathbf{q}}_v) \\ & + \bar{\mathbf{A}}(\mathbf{b}_a - \hat{\mathbf{b}}_a) + \bar{\mathbf{A}}\boldsymbol{\epsilon}_a. \end{aligned} \quad (17)$$

In order to avoid introducing new variable, let us redefine

$$\mathbf{x} = [\mathbf{r}^T \ \dot{\mathbf{r}}^T \ \tilde{\mathbf{q}}_v^T \ \mathbf{b}_g^T \ \mathbf{b}_a^T \ \boldsymbol{\rho}_1^T \ \boldsymbol{\rho}_2^T]^T, \quad (18)$$

to be the state vector of the KF estimator. Then, setting (7), (15), and (17) in the state-space form, the linearized model of the continuous system can be derived as

$$\delta\dot{\mathbf{x}} = \mathbf{F}\delta\mathbf{x} + \mathbf{G}\boldsymbol{\epsilon} \quad (19a)$$

where

$$\mathbf{F} = \begin{bmatrix} \mathbf{0} & \mathbf{I} & \mathbf{0} & \mathbf{0} & \mathbf{0} & \mathbf{0} \\ \mathbf{\Gamma} & -2\mathbf{n}[\mathbf{k} \times] & -2\bar{\mathbf{A}}[(\hat{\mathbf{u}}_a + \hat{\mathbf{b}}_a) \times] & \bar{\mathbf{A}} & \mathbf{0} & \mathbf{0} \\ \mathbf{0} & \mathbf{0} & -[(\hat{\mathbf{u}}_g + \hat{\mathbf{b}}_g) \times] & \mathbf{0} & \frac{1}{2}\mathbf{I} & \mathbf{0} \\ \mathbf{0} & \mathbf{0} & \mathbf{0} & \mathbf{0} & \mathbf{0} & \mathbf{0} \end{bmatrix} \quad (19b)$$

$$\mathbf{G} = \begin{bmatrix} \mathbf{0} & \mathbf{0} & \mathbf{0} \\ \bar{\mathbf{A}} & \mathbf{0} & \mathbf{0} \\ \mathbf{0} & \frac{1}{2}\mathbf{I} & \mathbf{0} \\ \mathbf{0} & \mathbf{0} & \mathbf{I} \\ \mathbf{0} & \mathbf{0} & \mathbf{0} \end{bmatrix} \quad (19c)$$

The equivalent discrete-time system of the linearized system can be written as

$$\delta\mathbf{x}_{k+1} = \Phi_k\delta\mathbf{x}_k + \mathbf{w}_k, \quad (20)$$

where \mathbf{w}_k is discrete-time process noise, and the state transition matrix $\Phi_k = \Phi(t_k, t_\Delta)$ at time t_k over time interval $t_\Delta = t_{k+1} - t_k$ is given by

$$\Phi(t_k, t_\Delta) = e^{\mathbf{F}(t_k)t_\Delta} \approx \mathbf{I} + t_\Delta\mathbf{F}(t_k). \quad (21)$$

The covariance of the discrete-time process noise is related to the continuous process noise covariance by

$$\mathbf{Q}_k = E[\mathbf{w}_k\mathbf{w}_k^T] = \int_{t_k}^{t_k+t_\Delta} \Phi(t_k, \tau)\mathbf{G}\boldsymbol{\Sigma}_{\text{IMU}}\mathbf{G}^T\Phi^T(t_k, \tau)d\tau, \quad (22)$$

Subsequently using the first-order approximation of the exponential matrix from (21) together with the expression of \mathbf{F} and \mathbf{G} from (19b) and (19c) into (22) and then carrying out tedious calculation of the integral, we arrive at the expression of the covariance matrix in the following form

$$\mathbf{Q}_k = \begin{bmatrix} \mathbf{Q}_{k11} & \mathbf{Q}_{k12} & \mathbf{0} & \mathbf{0} & \mathbf{0} \\ \times & \mathbf{Q}_{k22} & \mathbf{Q}_{k23} & \mathbf{Q}_{k24} & \mathbf{0} \\ \times & \times & \mathbf{Q}_{k33} & \mathbf{0} & \mathbf{0} \\ \times & \times & \times & \mathbf{Q}_{k44} & \mathbf{0} \\ \times & \times & \times & \times & \mathbf{0} \end{bmatrix}, \quad (23a)$$

where the sub-matrices are

$$\mathbf{Q}_{k11} = \frac{1}{3}\sigma_a^2 t_\Delta^3 \mathbf{I} \quad (23b)$$

$$\mathbf{Q}_{k12} = \sigma_a^2 \left(\frac{1}{2} t_\Delta^2 \mathbf{I} + \frac{2}{3} t_\Delta^3 n [\mathbf{k} \times] \right) \quad (23c)$$

$$\begin{aligned} \mathbf{Q}_{k22} &= \sigma_a^2 \left(t_\Delta \mathbf{I} - \frac{4}{3} t_\Delta^3 n^2 [\mathbf{k} \times]^2 \right) + \frac{1}{3} \sigma_b^2 t_\Delta^3 \mathbf{I} \\ &\quad - \frac{1}{3} \sigma_g^2 t_\Delta^3 \bar{\mathbf{A}}_k [(\hat{\mathbf{u}}_{a_k} + \hat{\mathbf{b}}_{a_k}) \times]^2 \bar{\mathbf{A}}_k^T \end{aligned} \quad (23d)$$

$$\begin{aligned} \mathbf{Q}_{k23} &= \sigma_g^2 \bar{\mathbf{A}}_k \left(\frac{1}{6} t_\Delta^3 [(\hat{\mathbf{u}}_{a_k} + \hat{\mathbf{b}}_{a_k}) \times][(\hat{\mathbf{u}}_{g_k} + \hat{\mathbf{b}}_{g_k}) \times] \right. \\ &\quad \left. + \frac{1}{4} t_\Delta [(\hat{\mathbf{u}}_{a_k} + \hat{\mathbf{b}}_{a_k}) \times] \right) \end{aligned} \quad (23e)$$

$$\mathbf{Q}_{k24} = \frac{1}{4} \sigma_b^2 t_\Delta^2 \bar{\mathbf{A}}_k \quad (23f)$$

$$\mathbf{Q}_{k33} = \sigma_g^2 \left(\frac{1}{4} t_\Delta \mathbf{I} - \frac{1}{12} t_\Delta^3 [(\hat{\mathbf{u}}_{g_k} + \hat{\mathbf{b}}_{g_k}) \times]^2 \right) \quad (23g)$$

$$\mathbf{Q}_{k44} = \sigma_b^2 t_\Delta \mathbf{I}. \quad (23h)$$

Notice that since the covariance matrix is symmetric, the sub-matrices in lower triangular part of \mathbf{Q}_k , which are denoted by the cross signs, are transposes of the corresponding sub-matrices in the upper triangular part. The process noise covariance matrix can be systematically calculated in (23) from where a priori knowledge of the IMU noise parameters $\{\sigma_a, \sigma_g, \sigma_b\}$, which are usually specified by the manufacturer. However, we treat them as the filter's "tuning parameters" to capture the linearization errors so that confidence in the linearized model can be properly specified [50].

Alternatively, the exact solution to the state transition matrix and discrete-time process noise can be obtained from the van Loan method [51] through the following steps: i) Construct upper triangular matrix $\mathbf{\Lambda}$ from (19b) and (19c) and then compute the exponential matrix $\mathbf{\Psi}$

$$\mathbf{\Lambda} \triangleq \begin{bmatrix} -\mathbf{F} & \mathbf{G}\Sigma_{\text{IMU}}\mathbf{G}^T \\ \mathbf{0} & \mathbf{F}^T \end{bmatrix}, \quad \mathbf{\Psi} = e^{\mathbf{\Lambda}t_\Delta}$$

with t_Δ being the sampling time; ii) partition the resultant upper-triangular matrix $\mathbf{\Psi}$ into sub-matrices $\mathbf{\Psi}_{11}$, $\mathbf{\Psi}_{12}$, and $\mathbf{\Psi}_{22}$ for construction of $\mathbf{\Phi}_k$ and \mathbf{Q}_k

$$\mathbf{\Psi} = \begin{bmatrix} \mathbf{\Psi}_{11} & \mathbf{\Psi}_{12} \\ \mathbf{0} & \mathbf{\Psi}_{22} \end{bmatrix} \implies \mathbf{\Phi}_k = \mathbf{\Psi}_{22}^T, \quad \mathbf{Q}_k = \mathbf{\Psi}_{22}^T \mathbf{\Psi}_{12} \quad (24)$$

Note that although (24) yields more accurate results than formulation (21)-(23), the latter does not require computation of exponential matrix and hence it is superior numerically to the former.

2.2 Observation Equations

As will be discussed later in Section 3, a noisy measurement of the relative pose can be obtained from registration of two 3-D point sets in the ICP algorithm. Assume that $\boldsymbol{\rho}'$ and \mathbf{q}' , respectively, represent the position and orientation parts of the rigid-body transformation at the end of the fine-alignment step of the data registration. Then similar to (14), one can transform the measured quaternion into small quaternion variation $\tilde{\mathbf{q}}' = \mathbf{q}' \otimes \bar{\mathbf{q}}^*$, and

$$\tilde{\mathbf{q}}'_v = \boldsymbol{\Lambda}(\bar{\mathbf{q}})\mathbf{q}', \quad \text{where} \quad \boldsymbol{\Lambda}(\bar{\mathbf{q}}) = [\bar{q}_o \mathbf{I} - [\bar{\mathbf{q}}_v \times] \quad -\bar{\mathbf{q}}_v]$$

Therefore, the observation vector is given by

$$\mathbf{z} = \begin{bmatrix} \boldsymbol{\rho}' \\ \boldsymbol{\Lambda}(\bar{\mathbf{q}})\mathbf{q}' \end{bmatrix}. \quad (25)$$

On the other hand, the observation equation can be written as a function of the state vector

$$\mathbf{z} = \mathbf{h}(\mathbf{x}) + \mathbf{v}, \quad (26)$$

where \mathbf{v} is the observation noise and the corresponding covariance $E[\mathbf{v}\mathbf{v}^T] = \mathbf{R}$ is allowed to be time-varying. The observation variables can be expressed in terms of the states variables as follows

$$\mathbf{h}(\mathbf{x}) = \begin{bmatrix} \mathbf{A}^T(\tilde{\mathbf{q}} \otimes \bar{\mathbf{q}})(\mathbf{r} - \boldsymbol{\rho}_2) + \boldsymbol{\rho}_1 \\ \tilde{\mathbf{q}}_v \end{bmatrix}. \quad (27)$$

Note that the observation vector (27) is a nonlinear function of the states. In view of (16), we can linearize the range measurement equation (2) in terms of $\tilde{\mathbf{q}}$ as follow

$$\boldsymbol{\rho} \approx (\mathbf{I} - 2[\tilde{\mathbf{q}}_v \times])\bar{\mathbf{A}}^T(\mathbf{r} - \boldsymbol{\rho}_2) + \boldsymbol{\rho}_1. \quad (28)$$

Therefore, we can write the sensitivity matrix as

$$\begin{aligned} \mathbf{H}_k &= \left. \frac{\partial \mathbf{h}}{\partial \mathbf{x}} \right|_{\bar{\mathbf{x}}_k} \\ &= \begin{bmatrix} \bar{\mathbf{A}}_k^T & \mathbf{0} & 2[(\bar{\mathbf{A}}_k^T(\bar{\mathbf{r}}_k - \bar{\boldsymbol{\rho}}_{2_k})) \times] & \mathbf{0} & \mathbf{0} & \mathbf{I} & -\bar{\mathbf{A}}_k^T \\ \mathbf{0} & \mathbf{0} & \mathbf{I} & \mathbf{0} & \mathbf{0} & \mathbf{0} & \mathbf{0} \end{bmatrix} \end{aligned} \quad (29)$$

Now, with the state transition matrix and the observation sensitivity matrix in hand, one can design the estimator as elaborated in Appendix A.

2.3 Estimation of the Observation Covariance Matrix

Efficient implementation of the KF requires the statistical characteristics of observation error in the innovation sequence of the filter [17]. The observation error is related to the pose

refinement step of ICP that depends on not only the quality of the 3D data acquired by the laser scanner, e.g., noise and outliers, but also the performance of ICP to converge to global minima. Unexpected noise and disturbance in the laser range sensor is largely responsible for the ICP error and thus a priori knowledge of the corresponding covariance is not usually available. Therefore, in order to improve the quality of the pose estimate requires weighting the ICP output with the proper data more heavily than the one with “poor” data in the estimator; rather than giving all ICP outputs equal weights. This goal can be achieved by readjusting the observation covariance matrix in the filter’s internal model, so that the filter is tuned as much as possible. In a noise-adaptive Kalman filter, the issue is that, in addition to the states, the covariance of the observation noise has to be estimated [52]. Adaptive Kalman filter based on *maximum likelihood estimation* was originally proposed by Mehra [53] followed by derivation of several variations and investigation of stability analysis [54, 55, 56]. The covariance matrix of the observation can be obtained from averaging the sequence of either the innovation matrix or the residual matrix inside a moving window of size w . Let us define the *innovation sequence* \mathbf{e}_k as the difference between incoming pose update from ICP loop \mathbf{z}_k and the predicted pose obtained from the *a priori* state estimate $\bar{\mathbf{x}}_k$, i.e.,

$$\mathbf{e}_k = \mathbf{z}_k - \mathbf{H}_k \bar{\mathbf{x}}_k \quad (30a)$$

$$= \mathbf{H}_k (\mathbf{x}_k - \bar{\mathbf{x}}_k) + \mathbf{v}_k. \quad (30b)$$

If we assume the estimation process remains constant over the most recent w steps, we can arrive estimate at estimation of the observation covariance by taking variance of both sides of (30b)

$$\frac{1}{w} \sum_{i=1}^w \mathbf{e}_{k-i} \mathbf{e}_{k-i}^T = \mathbf{H}_k \bar{\mathbf{P}}_k \mathbf{H}_k^T + \hat{\mathbf{R}}_k$$

or

$$\hat{\mathbf{R}}_k \approx \hat{\mathbf{C}}_k - \mathbf{H}_k \bar{\mathbf{P}}_k \mathbf{H}_k^T \quad (31a)$$

where

$$\hat{\mathbf{C}}_k = \frac{1}{w} \sum_{i=k-w}^{k-1} \mathbf{e}_i \mathbf{e}_i^T \quad (31b)$$

is the *innovation covariance matrix* averaged inside the sliding estimation window, and covariance of the predicted state vector $\bar{\mathbf{P}}_k = E[(\mathbf{x}_k - \bar{\mathbf{x}}_k)(\mathbf{x}_k - \bar{\mathbf{x}}_k)^T]$ is assumed constant within the window.

An alternative estimate of the observation covariance can be derived from the residual sequence instead of the innovation sequence. Let us define the *residual sequence*

$$\mathbf{e}_k^* = \mathbf{z}_k - \mathbf{H}_k \hat{\mathbf{x}}_k \quad (32)$$

as the difference between the observed pose and the estimated one obtained from *a priori* state estimate $\hat{\mathbf{x}}_k$. Then, it can be shown that expression of the estimated observation covariance takes the following form [54] similar to (31a)

$$\hat{\mathbf{R}}_k \approx \hat{\mathbf{C}}_k^* + \mathbf{H}_k \hat{\mathbf{P}}_k \mathbf{H}_k^T \quad (33a)$$

where the *innovation covariance matrix* is:

$$\hat{\mathbf{C}}_k^* = \frac{1}{w} \sum_{i=1}^w \mathbf{e}_{k-i}^* \mathbf{e}_{k-i}^{*T} \quad (33b)$$

Either formulation (31) or (33) can be used for estimation of the observation covariance matrix $\hat{\mathbf{R}}_k$ from an *ergodic* approximation of the covariance of the corresponding error in the sliding sampling window with finite length w . Nevertheless, only expression (33) guarantees that the outcome observation covariance matrix remains always positive-definite [57]. It should be pointed out that w has to be chosen empirically to give some statistical smoothing. The intuitive motion in choosing a finite window in the estimation of the innovation covariance matrix is that very past error data has to be discounted when being used for estimation of the current covariance. If the innovation covariance is not expected to change significantly over time, then a large sample size can be chosen for accurate estimation of the covariance matrix, otherwise the window should be selected as small as possible.

The recursive version of the innovation-based or the residual-based covariance estimation can be derived as following

$$\hat{\mathbf{C}}_{k+1} = \begin{cases} \frac{k-1}{k} \hat{\mathbf{C}}_k + \frac{1}{k} \mathbf{e}_k \mathbf{e}_k^T & \text{if } k < w \\ \hat{\mathbf{C}}_k + \frac{1}{w} (\mathbf{e}_k \mathbf{e}_k^T - \mathbf{e}_{k-w} \mathbf{e}_{k-w}^T) & \text{otherwise} \end{cases} \quad (34)$$

Note that $\hat{\mathbf{C}}$ and \mathbf{e} can be replaced by $\hat{\mathbf{C}}^*$ and \mathbf{e}^* in (34) for recursive representation of the residual-based method. The following block diagram illustrates the realization of the above recursive estimator for on-line estimation of the innovation covariance matrix. Here, $\text{covx}(\mathbf{a}) =$

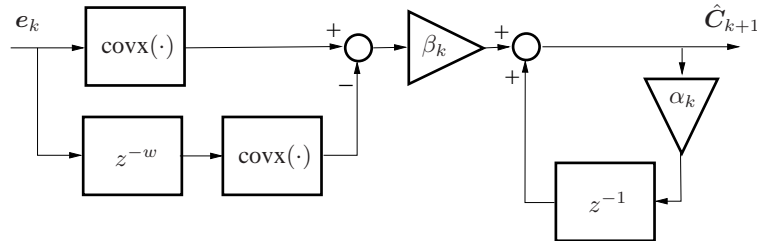


Figure 2: Online estimation of the innovation covariance.

$\mathbf{a}\mathbf{a}^T$, z^{-1} block represents *unit delay* and hence z^{-w} block represents w cascaded unit delay, and time-varying scaler variables α_k and β_k are defined as

$$\alpha_k = \begin{cases} \frac{k-1}{k} & \text{if } k < w \\ 1 & \text{otherwise} \end{cases}, \quad \beta_k = \begin{cases} \frac{1}{k} & \text{if } k < w \\ \frac{1}{w} & \text{otherwise} \end{cases}$$

We assume that the initial states of the memory block z^{-w} are zero while the output of memory block z^{-1} is specified as initial guess \mathbf{C}_0 for the first time.

3 Registration of two 3-D data points

Although the registration process of 3D CAD model and point cloud has been used by 3D vision algorithms for more than two decades, robust registration of two 3D point sets is still

a common problem in computer vision [58]. The iterative closest point (ICP) algorithm is the most popular algorithm for solving this kind of problem. Although there are many variants of the ICP algorithm, the basic ICP estimates the pose of an object in two steps as follows:

Step I: Find the corresponding points on the model set assuming a coarse alignment is given. Suppose that we are given with a set of 3-D points data \mathcal{C} that corresponds to a single shape represented by *model set* \mathcal{M} , which is usually a CAD model. It is known that for each point $\mathbf{c}_i \in \mathbb{R}^3$ from the 3-D points data set $\mathcal{C} = \{\mathbf{c}_1 \cdots \mathbf{c}_m\}$, there exists at least one point on the surface of \mathcal{M} which is closer to \mathbf{c}_i than other points in \mathcal{M} [59]. Assume that the initial rigid transformation $\{\mathbf{q}'(0), \boldsymbol{\rho}'(0)\}$ is given from prediction of the states at the propagation step of KF through the followings:

$$\begin{aligned} \mathbf{q}'(0) &= \bar{\mathbf{q}}_k \\ \boldsymbol{\rho}'(0) &= \mathbf{A}^T(\bar{\mathbf{q}}_k)(\bar{\mathbf{r}}_k - \bar{\boldsymbol{\rho}}_{2k}) + \bar{\boldsymbol{\rho}}_{k_1} \end{aligned} \quad (35a)$$

Then, the problem of finding the correspondence between the two sets can be formally expressed by

$$\mathbf{d}_i = \arg \min_{\mathbf{d}_j \in \mathcal{M}} \|\mathbf{A}(\mathbf{q}'(0))\mathbf{c}_i + \boldsymbol{\rho}'(0) - \mathbf{d}_j\| \quad \forall i = 1, \dots, m, \quad (36)$$

and subsequently set $\mathcal{D} = \{\mathbf{d}_1 \cdots \mathbf{d}_m\}$ is formed. Now, we have two independent sets of 3-D points \mathcal{C} and \mathcal{D} both of which corresponds to a single shape but they are related to each other through a rigid-body transformation.

Step II: Finding a fine-alignment between two data sets. The next problem is to find a fine-alignment $[\boldsymbol{\rho}^T \mathbf{q}^T]^T$ which minimizes the distance between these two sets of points [34]. This can be formally formulated as

$$\begin{aligned} \varepsilon &= \arg \min_{\mathbf{q}, \boldsymbol{\rho}} \frac{1}{m} \sum_{i=1}^m \|\mathbf{A}(\mathbf{q})\mathbf{c}_i + \boldsymbol{\rho} - \mathbf{d}_i\|^2 \quad \forall \mathbf{d}_i \in \mathcal{D}, \mathbf{c}_i \in \mathcal{C} \\ \text{s.t.} \quad &\|\mathbf{q}\| = 1 \end{aligned} \quad (37)$$

where ε is called ICP metric fit error. There are several closed-form solutions to the above least-squares minimization problem [60, 61], of which the quaternion-based algorithm is the preferable choice for $m > 3$ over other methods [62, 34]. Consider the cross-covariance matrix of the sets \mathcal{C} and \mathcal{D} given by

$$\mathbf{S} = \text{cov}(\mathcal{C}, \mathcal{D}) = \frac{1}{m} \sum_i \mathbf{c}_i \mathbf{d}_i^T - \bar{\mathbf{c}} \bar{\mathbf{d}}^T \quad (38)$$

where $\bar{\mathbf{c}} = \frac{1}{m} \sum_i \mathbf{c}_i$ and $\bar{\mathbf{d}} = \frac{1}{m} \sum_i \mathbf{d}_i$ are the corresponding centroid of the sets. Let us construct the following symmetric weighting matrix from cross-covariance matrix as follow

$$\mathbf{W} = \begin{bmatrix} \text{tr}(\mathbf{S}) & \mathbf{s}^T \\ \mathbf{s} & \mathbf{S} + \mathbf{S}^T - \text{tr}(\mathbf{S})\mathbf{I} \end{bmatrix},$$

where $\mathbf{s} = [S_{23} - S_{32}, S_{31} - S_{13}, S_{12} - S_{21}]^T$. Then, it has shown that minimization problem (37) is tantamount to find the solution of following quadratic programming [62]

$$\max_{\|\mathbf{q}\|=1} \mathbf{q}^T \mathbf{W} \mathbf{q} \quad (39)$$

As shown in Appendix B, the solution of the preceding optimization problem is

$$\mathbf{q}' = \underset{\lambda_{\max}(\mathbf{W})}{\text{eigenvector}}(\mathbf{W}) \quad (40)$$

That is the eigenvector corresponding to the largest eigenvalue of matrix \mathbf{W} . Then, the translation can be obtained from

$$\boldsymbol{\rho}' = \bar{\mathbf{d}} - \mathbf{A}(\mathbf{q}')\bar{\mathbf{c}} \quad (41)$$

It should be mentioned that there is also a preprocessing step in the registration process where the 3D CAD model is converted into suitable representation for the ICP. The 3D CAD model is often exported into *stereolithography* (STL) format consisting of normal and triangular facets, which are then used as a biases to generate a point cloud model with uniform resolution. Generally speaking, the point cloud obtained from the CAD model should have comparable resolutions with the one acquired by the laser scanner in order to maintain accurate registration results [63]. Therefore, re-sampling of model points may be required as the resolution of the scanned point data set depends on the distance between the scanner sensor and the object. In our application, the point cloud model is generated once for use in all ICP cycles for the sake of simplicity of implementation. Nevertheless, the model points can be subject to a data re-sampling process using different methods as discussed in [64].

In the conventional ICP approaches, the incremental transformation obtained from the fine-alignment step is applied to step I and then it is iterated until the distance between the two sets of points in (37) is less than the pre-specified threshold ε_{th} . As illustrated in Algorithm 1, however, the process of our robust pose estimation algorithm follows these steps: If the ICP matching error ε becomes lower than the threshold ε_{th} before the maximum number of iterations i_{max} is reached, then ICP iteration is considered convergent. In this case, the rigid-body transformation obtained from the refinement step, i.e., (40) and (41), is used not only to correct state estimation in the KF innovation sequence but to update covariances of state estimation and observation error (45). Subsequently, a posteriori values of the state vector and the state covariance matrix are computed through the propagation step (46). The predicated pose is set as the coarse alignment to find the corresponding points (step I of ICP) in the next time step as described in (35). On the other hand, if $\varepsilon > \varepsilon_{\text{th}}$ but the maximum number of iteration is not reached, then the rigid-body transformation obtained from (40) and (41) is used to set the initial pose and the iterations are carried out at the current time step. Finally, if the maximum number of iteration is reached while the data set matching error is still not below the threshold ε_{th} , then the ICP iteration is considered a failure and subsequently the *a priori* state estimation is used to compute pose estimate.

Suppose the following flagged variable indicates whether the 3D registration process at epoch k is healthy or faulty

$$\phi_k = \begin{cases} 0 & \text{ICP fault} \\ 1 & \text{Otherwise} \end{cases} \quad (42)$$

As mentioned earlier, a large ICP metric fit error indicates non-convergent ICP and that is at the core of our fault-detection mechanism. However, even convergent ICP does not always guarantee that the pose estimation outcome is valid. This is because even if the metric error becomes relatively small, it is still possible to get erroneous results due to multiple effects such as sensor noise, outliers, or convergence to local minima. The validity of the ICP pose

estimation outcome can be examined by comparing it with the predicted pose derived from the dynamics model and using acceleration and rotation data measured by IMU. A significant mismatch then can be also interpreted as ICP fault. Therefore, the condition for detecting ICP fault can be expanded as

$$\varepsilon \geq \varepsilon_{\text{th}} \quad \text{or} \quad \|\mathbf{e}_k\|_W \geq e_{\text{th}}, \quad (43)$$

where \mathbf{e}_k is difference between ICP pose estimate and pose predication based on the *a priori* state estimate (30a), e_{th} is the pose error threshold, and $\|\cdot\|_W$ denotes weighted Euclidian norm. Once ICP fault is detected, the pose-tracking fault recovery is rather straightforward. To this end, the Kalman filter gain is set to

$$\mathbf{K}_k = \phi_k \bar{\mathbf{P}}_k \mathbf{H}_k^T \hat{\mathbf{C}}_k^{-1} \quad (44)$$

Clearly $\mathbf{K}_k = \mathbf{0}$ when ICP fault is detected, in which case the observation information is not incorporated in the estimation process for updating the state and the estimator covariance, i.e., $\phi_k = 0 \implies \hat{\mathbf{x}}_k = \bar{\mathbf{x}}_k, \hat{\mathbf{P}}_k = \bar{\mathbf{P}}_k$.

Algorithm 1: ICP-AKF INTEGRATION

Input: measurements $\mathcal{C}_k = \{\mathbf{c}_{1k}, \dots, \mathbf{c}_{m_k}\}$, \mathbf{u}_k
Output: Pose estimate

- 1 $i \leftarrow 0$
- 2 **while** $i < i_{\text{max}}$ **do**
- 3 $i \leftarrow i + 1$
- 4 ICP step I: $\mathcal{D} = \{\mathbf{d}_1, \dots, \mathbf{d}_m\} \leftarrow \mathbf{q}'(0), \boldsymbol{\rho}'(0), \mathcal{C}_k$
- 5 ICP step II: $\{\mathbf{q}', \boldsymbol{\rho}', \varepsilon\} \leftarrow \mathcal{D}, \mathcal{C}_k$
- 6 **if** $\varepsilon \leq \varepsilon_{\text{th}}$ **then**
- 7 Innovation sequence: $\{\hat{\mathbf{q}}_k, \hat{\boldsymbol{\rho}}_k, \hat{\mathbf{x}}_k\} \leftarrow \{\mathbf{q}', \boldsymbol{\rho}'\}$
- 8 Update covariance: $\hat{\mathbf{C}}_k \leftarrow \{\hat{\mathbf{e}}_k \hat{\mathbf{e}}_k^T, \hat{\mathbf{C}}_{k-1}\}$
- 9 Propagation sequence: $\{\bar{\mathbf{q}}_{k+1}, \bar{\boldsymbol{\rho}}_{k+1}, \bar{\mathbf{x}}_{k+1}, \bar{\mathbf{P}}_{k+1}\} \leftarrow \{\hat{\mathbf{x}}_k, \mathbf{u}_k, \hat{\mathbf{P}}_k\}$
- 10 $\mathbf{q}'(0) \leftarrow \bar{\mathbf{q}}_{k+1} \quad \wedge \quad \boldsymbol{\rho}'(0) \leftarrow \bar{\boldsymbol{\rho}}_{k+1}$
- 11 $\phi_k \leftarrow 1$
- 12 **return** $\hat{\mathbf{q}}_k, \hat{\boldsymbol{\rho}}_k, \phi_k$
- 13 **else**
- 14 $\mathbf{q}'(0) \leftarrow \mathbf{q}' \quad \wedge \quad \boldsymbol{\rho}'(0) \leftarrow \boldsymbol{\rho}'$
- 15 Update: $\hat{\mathbf{x}}_k \leftarrow \bar{\mathbf{x}}_k, \hat{\mathbf{C}}_k \leftarrow \hat{\mathbf{C}}_{k-1}, \hat{\mathbf{P}}_k \leftarrow \bar{\mathbf{P}}_k$
- 16 Propagation sequence: $\{\bar{\mathbf{q}}_{k+1}, \bar{\boldsymbol{\rho}}_{k+1}, \bar{\mathbf{x}}_{k+1}, \bar{\mathbf{P}}_{k+1}\} \leftarrow \{\hat{\mathbf{x}}_k, \mathbf{u}_k, \hat{\mathbf{P}}_k\}$
- 17 $\mathbf{q}'(0) \leftarrow \bar{\mathbf{q}}_{k+1} \quad \wedge \quad \boldsymbol{\rho}'(0) \leftarrow \bar{\boldsymbol{\rho}}_{k+1}$
- 18 $\phi_k \leftarrow 0$
- 19 **return** $\hat{\mathbf{q}}_k, \hat{\boldsymbol{\rho}}_k, \phi_k$

Appendix A: Noise adaptive Kalman filter

The Kalman-based observer for the associated linearized system (19)-(29) is given in the following steps:

i. Update:

$$\mathbf{K}_k = \phi_k \bar{\mathbf{P}}_k \mathbf{H}_k^T \hat{\mathbf{C}}_k^{-1} \quad (45a)$$

$$\hat{\mathbf{x}}_k = \bar{\mathbf{x}}_k + \mathbf{K}_k (\mathbf{z}_k - \mathbf{h}(\bar{\mathbf{x}}_k)) \quad (45b)$$

$$\hat{\mathbf{q}}_k = \hat{\bar{\mathbf{q}}}_k \otimes \bar{\mathbf{q}}_k \quad (45c)$$

$$\hat{\mathbf{P}}_k = (\mathbf{I} - \mathbf{K}_k \mathbf{H}_k) \bar{\mathbf{P}}_k \quad (45d)$$

ii. On-line estimation of the covariance matrix from (34)

iii. Propagation:

$$\bar{\mathbf{x}}_{k+1} = \hat{\mathbf{x}}_k + \int_{t_k}^{t_k+t_\Delta} \mathbf{f}(\mathbf{x}, \mathbf{u}(\tau), \mathbf{0}) d\tau \quad (46a)$$

$$\bar{\mathbf{P}}_{k+1} = \hat{\Phi}_k \mathbf{P}_k \hat{\Phi}_k^T + \mathbf{Q}_k \quad (46b)$$

For non-adaptive KF, the covariance matrix on the innovation can be constructed from a given covariance matrix of the vision system noise by

$$\mathbf{C}_k = \mathbf{H}_k \bar{\mathbf{P}}_k \mathbf{H}_k^T + \mathbf{R}_k$$

Appendix B: Optimal quaternion estimate

Denote the Lagrangian equation of the constrained quadratic programming (39) as

$$L = \mathbf{q}^T \mathbf{W} \mathbf{q} - \lambda (\mathbf{q}^T \mathbf{q} - 1)$$

where λ is the Lagrangian multiplier. Then, the optimal solution has to satisfy the stationary condition, which leads to the following equation:

$$\frac{\partial L}{\partial \mathbf{q}} = 0 \quad \Rightarrow \quad \mathbf{W} \mathbf{q} - \lambda_{\max} \mathbf{q} = \mathbf{0} \quad (47)$$

Notice that (47) is indeed equivalent to the characteristic equation of matrix \mathbf{W} for the largest eigenvalue $\lambda_{\max} = \lambda_{\max}(\mathbf{W})$. In other words, the optimal quaternion is the eigenvector of matrix \mathbf{W} corresponding to its largest eigenvalue.

References

- [1] F. Aghili and C. Y. Su, "Robust relative navigation by integration of icp and adaptive kalman filter using laser scanner and imu," *IEEE/ASME Transactions on Mechatronics*, vol. 21, no. 4, pp. 2015–2026, Aug 2016.
- [2] G. M. Hoffmann, D. Gorinevsky, R. W. Mah, C. J. Tomlin, and J. D. Mitchell, "Fault tolerant relative navigation using inertial and relative sensors," in *Proc. of the AIAA Space 2000 Conference*, Hilton Head, South Carolina, USA, 20–27 August 2007.

- [3] F. Aghili, “Fault-tolerant and adaptive visual servoing for capturing moving objects,” *IEEE/ASME Transactions on Mechatronics*, vol. 27, no. 3, pp. 1773–1783, 2022.
- [4] B. A. Kriegsman, “Radar-updated inertial navigation of a continuously-powered space vehicle,” *Aerospace and Electronic Systems, IEEE Transactions on*, vol. AES-2, no. 4, pp. 549–565, July 1966.
- [5] A. Emadzadeh and J. Speyer, “Relative navigation between two spacecraft using x-ray pulsars,” *Control Systems Technology, IEEE Transactions on*, vol. 19, no. 5, pp. 1021–1035, Sept 2011.
- [6] F. Aghili, “Optimal post-grasping robotic maneuvers for stabilization of a tumbling satellite,” *AIAA Journal of Guidance, Control, and Dynamics*, vol. 43, no. 10, p. 1952–1959, 2020.
- [7] J. Liu, J. Fang, X. Ma, Z. Kang, and J. Wu, “X-ray pulsar/starlight doppler integrated navigation for formation flight with ephemerides errors,” *Aerospace and Electronic Systems Magazine, IEEE*, vol. 30, no. 3, pp. 30–39, March 2015.
- [8] F. Aghili, “Active orbital debris removal using space robotics,” in *International Symposium on Artificial Intelligence, Robotics and Automation in Space i-SAIRAS*, Turin, Italy, Sep. 4–6 2012.
- [9] F. Aghili, M. Kuryllo, G. Okouneva, and C. English, “Fault-tolerant position/attitude estimation of free-floating space objects using a laser range sensor,” *IEEE Sensors Journal*, vol. 11, no. 1, pp. 176–185, Jan. 2011.
- [10] T. Corazzini, A. Robertson, A. Adams, and J. C. Hassibi, “Gps sensing for spacecraft formation,” in *Proc. of ION-GPS*, Kansas City, MO, September 1997, pp. 735–744.
- [11] J. Wolfe and J. L. Speyer, “Effective estimation of relative positions in orbit using differential carrier-phase,” in *Proc. of the AIAA Guidance, Navigation and Control Conference*, Providence, Rhode Island, August 2004.
- [12] F. Aghili, “Pre- and post-grasping robot motion planning to capture and stabilize a tumbling/driftig free-floater with uncertain dynamics,” in *IEEE International Conf. on Robotics & Automation*, Karlsruhe, Germany, May 6–10 2013, pp. 5441–5448.
- [13] A. Almagbile, J. Wang, and W. Ding, “Evaluating the performance of adaptive kalman filter methods in gps/ins integration,” *Journal of Global Positioning Systems*, vol. 9, no. 1, pp. 33–40, 2010.
- [14] Y. Masutani, T. Iwatsu, and F. Miyazaki, “Motion estimation of unknown rigid body under no external forces and moments,” in *IEEE Int. Conf. on Robotics & Automation*, San Diego, May 1994, pp. 1066–1072.
- [15] C. Samson, C. English, A. Deslauriers, I. Christie, F. Blais, and F. Ferrie, “Neptec 3D laser camera system: From space mission STS-105 to terrestrial applications,” *Canadian Aeronautics and Space Journal*, vol. 50, no. 2, pp. 115–123, 2004.

- [16] M. Mokuno, I. Kawano, and T. Suzuki, “In-orbit demonstration of rendezvous laser radar for unmanned autonomous rendezvous docking,” *Aerospace and Electronic Systems, IEEE Transactions on*, vol. 40, no. 2, pp. 617–626, April 2004.
- [17] F. Aghili and K. Parsa, “An adaptive vision system for guidance of a robotic manipulator to capture a tumbling satellite with unknown dynamics,” in *IEEE/RSJ Int. Conf. on Intelligent Robots and Systems*, Nice, France, September 2008, pp. 3064–3071.
- [18] F. Aghili, “Optimal control for robotic capturing and passivation of a tumbling satellite with unknown dynamics,” in *AIAA Guidance, Navigation and Control Conference*, Honolulu, Hawaii, August 2008.
- [19] T. Shibata, Y. Matsumoto, T. Kuwahara, M. Inaba, and H. Inoue, “Development and integration of generic components for a teachable vision-based mobile robot,” *Mechatronics, IEEE/ASME Transactions on*, vol. 1, no. 3, pp. 230–236, Sept 1996.
- [20] F. Aghili, “A prediction and motion-planning scheme for visually guided robotic capturing of free-floating tumbling objects with uncertain dynamics,” *IEEE Transactions on Robotics*, vol. 28, no. 3, pp. 634–649, June 2012.
- [21] G. Lu and M. Tomizuka, “Lidar sensing for vehicle lateral guidance: Algorithm and experimental study,” *Mechatronics, IEEE/ASME Transactions on*, vol. 11, no. 6, pp. 653–660, Dec 2006.
- [22] J. Leavitt, A. Sideris, and J. Bobrow, “High bandwidth tilt measurement using low-cost sensors,” *Mechatronics, IEEE/ASME Transactions on*, vol. 11, no. 3, pp. 320–327, June 2006.
- [23] G. Fu, P. Corradi, A. Menciassi, and P. Dario, “An integrated triangulation laser scanner for obstacle detection of miniature mobile robots in indoor environment,” *Mechatronics, IEEE/ASME Transactions on*, vol. 16, no. 4, pp. 778–783, Aug 2011.
- [24] K. Wang, Y. hui Liu, and L. Li, “A simple and parallel algorithm for real-time robot localization by fusing monocular vision and odometry/ahrs sensors,” *Mechatronics, IEEE/ASME Transactions on*, vol. 19, no. 4, pp. 1447–1457, Aug 2014.
- [25] J. Simanek, M. Reinstein, and V. Kubelka, “Evaluation of the ekf-based estimation architectures for data fusion in mobile robots,” *Mechatronics, IEEE/ASME Transactions on*, vol. 20, no. 2, pp. 985–990, April 2015.
- [26] F. Aghili, “Automated rendezvous & docking (AR&D) without impact using a reliable 3d vision system,” in *AIAA Guidance, Navigation and Control Conference*, Toronto, Canada, August 2010.
- [27] C. English, S. Zhu, C. Smith, S. Ruel, and I. Christie, “TriDar: A hybrid sensor for exploiting the complementary nature of triangulation and lidar technologies,” in *International Symposium on Artificial Intelligence, Robotics and Automation in Space (ISAIRAS)*, Munich, Germany, 5-8 September 2005.

- [28] F. Aghili, K. Parsa, and E. Martin, “A vision-guided system for robotic capture of a tumbling satellite in presence of occlusion,” in *CISM-IFTOMM Symposium on Robot Design, Dynamics, and Control*, Tokyo, Japan, July 2008, pp. 3–10.
- [29] F. Aghili and K. Parsa, “Adaptive motion estimation of a tumbling satellite using laser-vision data with unknown noise characteristics,” in *2007 IEEE/RSJ International Conference on Intelligent Robots and Systems*, Oct 2007, pp. 839–846.
- [30] F. Aghili, K. Parsa, and E. Martin, “Robotic docking of a free-falling space object with occluded visual condition,” in *9th Int. Symp. on Artificial Intelligence, Robotics & Automation in Space*, Los Angeles, CA, Feb. 26 – 29 2008.
- [31] F. Aghili, M. Kuryllo, G. Okouneva, and C. English, “Fault-tolerant pose estimation of space objects,” in *IEEE/ASME Int. Conf. on Advanced Intelligent Mechatronics (AIM)*, Montreal, Canada, July 2010, pp. 947–954.
- [32] ———, “Robust vision-based pose estimation of moving objects for automated rendezvous & docking,” in *IEEE Int. Conf. on Mechatronics and Automation (ICMA)*, Xian, China, August 2010, pp. 305–311.
- [33] S.-H. Kim, Y.-H. Hwang, H. K. Hong, and M.-H. Choi, *Advances in Artificial Intelligence MICAI*. Berlin, Heidelberg: Springer, 2004, ch. An Improved ICP Algorithm Based on the Sensor Projection for Automatic 3D Registration, pp. 642–651.
- [34] P. J. Besl and N. D. McKay, “A method for registration of 3-D shapes,” *IEEE Trans. on Pattern Analysis & Machine Intelligence*, vol. 14, no. 2, pp. 239–256, 1992.
- [35] M. Greenspan and M. Yurick, “Approximate K-D tree search for efficient ICP,” in *IEEE International Conference on Recent Advances in 3D Digital Imaging and Modeling*, Banff, Canada, October 2003, pp. 442–448.
- [36] Y. Chen and G. G. Medioni, “Object modeling by registration of multiple range images,” *Image and Vision Computing*, vol. 10, no. 3, pp. 145–155, 1992.
- [37] S. Rusinkiewicz and M. Levoy, “Efficient variants of the ICP algorithm,” in *Proc. of 3rd Int. Conf. on 3-D Digital Imaging and Modeling*, Quebec City, Canada, 28 May – 1 June 2001, pp. 145–152.
- [38] G. Godin, D. Laurendeau, and R. Bergevin, “A method for the registration of attributed range images,” in *Proc. of 3rd Int. Conf. on 3-D Digital Imaging and Modeling*, Quebec City, Canada, 28 May – 1 June 2001, pp. 179–186.
- [39] S. Du, N. Zheng, S. Ying, and J. Liu, “Affine iterative closest point algorithm for point set registration,” *Pattern Recognition Letters*, vol. 31, no. 9, pp. 791–799, 2010.
- [40] J. Dong, Y. Peng, S. Ying, and Z. Hu, “Lietricp: An improvement of trimmed iterative closest point algorithm,” *Journal of Neurocomputing*, vol. 140, no. 22, pp. 67–76, September 2014.

- [41] W. Li, Z. Yin, Y. Huang, and Y. Xiong, “Three-dimensional point-based shape registration algorithm based on adaptive distance function,” *Computer Vision, IET*, vol. 5, no. 1, pp. 68–76, Jan 2011.
- [42] H. Pottmann, Q.-X. Hung, Y.-L. Yang, and S.-M. Hu, “Geometry and convergence analysis of algorithms for registration of 3d shapes,” *Int. Journal of Computer Vision*, vol. 67, no. 3, pp. 277–296, 2006.
- [43] W. Wang, H. Pottmann, and Y. Liu, “Fitting b-spline curves to point clouds by curvature-based squared distance minimization,” *ACM Trans. Graph.*, vol. 25, no. 2, pp. 214–238, 2006.
- [44] U. Hillenbrand and R. Lampariello, “Motion and parameter estimation of a free-floating space object from range data for motion prediction,” in *The 8th Int. Symposium on Artificial Intelligence, Robotics and Automation in Space: i-SAIRAS 2005*, Munich, Germany, Sep. 5–8 2005.
- [45] W. H. Clohessy and R. S. Wiltshire, “Terminal guidance system for satellite rendezvous,” *Journal of Aerospace Science*, vol. 27, no. 9, pp. 653–658, 1960.
- [46] E. J. Lefferts, F. L. Markley, and M. D. Shuster, “Kalman filtering for spacecraft attitude estimation,” vol. 5, no. 5, pp. 417–429, Sep.–Oct. 1982.
- [47] M. E. Pittelkau, “Kalman filtering for spacecraft system alignment calibration,” vol. 24, no. 6, pp. 1187–1195, Nov. 2001.
- [48] J. C. Wilcox, “A new algorithm for strapped-down inertial navigation,” *IEEE Trans. on Aerospace and Electronic Systems*, vol. 3, no. 5, pp. 796–802, Sep. 1967.
- [49] R. Zanetti, “Recursive update filtering for nonlinear estimation,” *Automatic Control, IEEE Transactions on*, vol. 57, no. 6, pp. 1481–1490, June 2012.
- [50] J. Valappil and C. Georgakis, “Systematic estimation of state noise statistics for extended kalman filters,” *AICHE Journal*, vol. 46, no. 2, pp. 292–308, Feb 2000.
- [51] C. F. van Loan, “Computing integrals involving the matrix exponential,” *IEEE Trans. on Automatic Control*, vol. 23, no. 3, pp. 396–404, Jun. 1978.
- [52] C. K. Chui and G. Chen, *Kalman Filtering with Real-Time Applications*. Berlin: Springer, 1998, pp. 113–115.
- [53] R. Mehra, “On the identification of variances and adaptive kalman filtering,” *Automatic Control, IEEE Transactions on*, vol. 15, no. 2, pp. 175–184, Apr 1970.
- [54] J. Wang, “Stochastic modeling for real-time kinematic gps/glonass position,” *Journal of Navigation*, vol. 46, no. 4, pp. 297–305, 2000.
- [55] K. Kim, G. Jee, C.-G. Park, and J.-G. Lee, “The stability analysis of the adaptive fading extended kalman filter using the innovation covariance,” *International Journal of Control, Automation and Systems*, vol. 7, no. 1, pp. 49–56, Feb 2009.

- [56] S. Gao, W. Wei, Y. Zhong, and A. Subic, “Sage windowing and random weighting adaptive filtering method for kinematic model error,” *Aerospace and Electronic Systems, IEEE Transactions on*, vol. 51, no. 2, pp. 1488–1500, April 2015.
- [57] F. Aghili and K. Parsa, “Motion and parameter estimation of space objects using laser-vision data,” *AIAA Journal of Guidance, Control, and Dynamics*, vol. 32, no. 2, pp. 538–550, March 2009.
- [58] L. Shang, P. Jasiobedzki, and M. Greenspan, “Discrete pose space estimation to improve icp-based tracking,” in *3-D Digital Imaging and Modeling, 2005. 3DIM 2005. Fifth International Conference on*, June 2005, pp. 523–530.
- [59] D. A. Simon, M. Herbert, and T. Kanade, “Real-time 3-d estimation using a high-speed range sensor,” in *IEEE Int. Conference on Robotics & Automation*, San Diego, CA, May 1994, pp. 2235–2241.
- [60] O. D. Faugeras and M. Herbert, “The representation, recognition, and locating of 3-d objects,” *The International Journal of Robotics Research*, vol. 5, no. 3, pp. 27–52, 1986.
- [61] D. Eggert, A. Lorusso, and R. B. Fisher, “Estimating 3-D rigid body transformation: a comparison of four major algorithms,” *Machine Vision & Applications*, vol. 9, no. 5, March 1997.
- [62] B. K. P. Horn, “Closed-form solution of absolute orientation using unit quaternions,” *J. Opt. Soc. Amer.*, vol. 4, no. 4, pp. 629–642, Apr. 1987.
- [63] Y. Z. H. Y. Li, W. and Y. Xiong, “Automatic registration for 3d shapes using hybrid dimensionality-reduction shape descriptions,” *Pattern Recognition*, vol. 44, no. 12, pp. 2926–2943, December 2011.
- [64] C. Kim, J. Lee, M. Cho, and C. Kim, “Fully automated registration of 3d cad model with point cloud from construction site,” in *Proceedings of the 28th International Symposium on Automation and Robotics in Construction*, Seoul, Korea, 29 June–2 July 2011, pp. 917–922.